River Flow 2014 – Schleiss et al. (Eds)
© 2014 Taylor & Francis Group, London, ISBN 978-1-138-02674-2

Bedload particle velocity in supercritical open channel flows

C. Auel, I. Albayrak & R.M. Boes
Laboratory of Hydraulics, Hydrology and Glaciology (VAW), ETH Zurich, Zurich, Switzerland

ABSTRACT: Single glass sphere motion recordings were conducted in a transitional-rough bed open channel at steady and highly supercritical flow similar to hydraulic conditions in sediment bypass tunnels. A high speed camera with a maximum resolution of 2,560 × 2,160 pixels was used to record the movement of bedload particles with diameters of D = 5.3, 10.3 and 17.5 mm. An in-house developed Particle Tracking Velocimetry (PTV) program was used to determine the transport mode and velocities of each particle for a wide range of Froude numbers up to F_o = 6. The relative roughness defined as the ratio of the bed roughness height k_s to the water depth h varied from k_s/h = 0.02–0.03. Particles were observed to move in rolling and saltation modes depending on the Shields number. The particle velocity shows a linearly increasing relationship with both friction velocity and Froude number nearly independent on the particle diameter. A linear relationship was also found between rolling and saltating particle velocities indicating that particle velocity does not depend on the transport mode in the range of the investigated hydraulic conditions. Scaling of particle velocity with the wave celerity plotted as a function of the Froude number adequately merged external data sets with the present data. As a consequence, a linear fit for a large Froude number range was obtained.

1 INTRODUCTION

Sediment bypass tunnels are operated in supercritical open channel flow. They provide an effective measure to decrease reservoir sedimentation by bypassing sediments into the dam tailwater during floods. Due to high flow velocities and sediment transport in these structures invert abrasion damages occur causing significant annual maintenance cost (Sumi et al. 2004, Auel & Boes 2011). The Laboratory of Hydraulics, Hydrology and Glaciology (VAW) of ETH Zurich initiated a research project to counter the invert abrasion and thus contribute to a sustainable use of bypass tunnels (Auel & Boes 2012). The main goals of the project are to investigate the (1) mean and turbulence characteristics (Auel et al. 2014a), (2) sediment motion and transport mode, and (3) relationship between the transport modes and rates, and the invert abrasion depth of supercritical open channel flows. This contribution focuses on the particle velocities of one test series as a partial result of phase (2).

Early laboratory investigations on particle motion and transport mode in turbulent open channel flows were carried out by Francis (1973), Abbott & Francis (1977), Murphy & Hooshiari (1982), and van Rijn (1984). They analyzed single particle saltation trajectories and particle velocities V_p. The particle velocity is essentially dependent on the fluid velocity U and the bed roughness height k_s. Particles are transported in either rolling, saltation or suspended motion. At low flow velocities, the main transport mode of a particle is rolling, and the particle velocity corresponds to the rolling velocity. With increasing flow intensity, i.e. Shields number θ, the mode shifts to saltation and the particle velocity corresponds to the saltation velocity. Abbott & Francis (1977), Niño et al. (1994), Hu & Hui (1996), Ancey et al. (2002) and Chatanantavet et al. (2013) focused on solely saltation mode and thus provided saltation particle velocities. Meland & Norrman (1966), Fernandez Luque & van Beek (1976), Ancey et al. (2003), and Julien & Bounvilay (2013) investigated bedload motion by focusing on the rolling velocity of a particle. General conclusions drawn from the above listed references are summarized as: (I) saltation velocities are slightly lower than fluid velocities, (II) rolling velocities are somewhat lower than saltation velocities for particle motion on a rough bed. In the case of particle motion over a smooth bed these differences decrease and the particle velocity approach to the value of the fluid velocity.

2 THEORETICAL MODEL

Particle motion in a water stream is driven by hydrodynamic forces. According to Murphy & Hooshiari (1982), van Rijn (1984) and Lee & Hsu (1994) the acting forces are the drag force F_D

caused by pressure and skin friction forces, the lift forces F_{LG} and F_{LS}, caused by the flow velocity gradient (shear effect) and the spinning motion of the particle (Magnus effect), respectively. The retarding forces are the gravitational weight G diminished by the buoyancy force F_B, and the added mass force due to particle acceleration F_{AM} (Fig. 1).

The drag is dependent on the slip velocity multiplied by the drag coefficient C_D:

$$F_D = \frac{1}{2}\rho A_D C_D \left(U - V_p\right)^2 \tag{1}$$

where ρ = fluid density, A_D = projected particle area perpendicular to the flow, U = the time averaged velocity measured in front of a particle, and V_p = particle velocity. The lift force F_{LG} is dependent on the difference between the fluid velocity at the top and bottom of the particle U_{top} and U_{bot} and follows as (Chepil 1958)

$$F_{LG} = \frac{1}{2}\rho A_L C_{LG}\left(U_{top}^2 - U_{bot}^2\right) \tag{2}$$

where A_L = projected particle area perpendicular to the flow. For a sphere the projected particle areas A_D and A_L are equal to $(\pi/4)D^2$, with D = particle diameter. The lift force F_{LS} due to the Magnus effect in a viscous flow is determined by Rubinow & Keller (1961):

$$F_{LS} = C_{LS}\rho D^3\left(U - V_p\right)\cdot\omega \tag{3}$$

where C_{LS} = lift coefficient for spinning motion, $\omega = 2\pi n_s$ = particle angular velocity, and n_s = spinning rate. However, F_{LS} is usually neglected in sediment transport related phenomena due to low particle angular velocities.

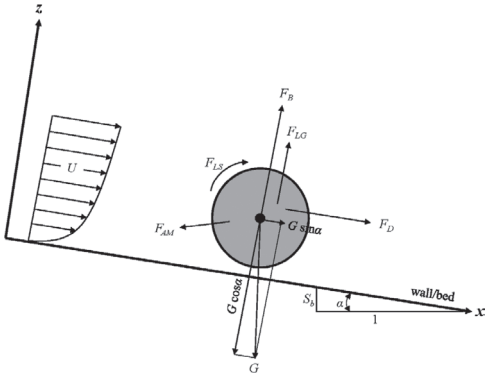

Figure 1. Sketch of acting forces on a particle in motion.

The gravitational and buoyancy force can be merged and rewritten as the submerged weight of the particle F_G as

$$F_G = G - F_B\cos\alpha = (s-1)\rho V_p g\cos\alpha \tag{4}$$

where $s = \rho_s/\rho$, with ρ_s = particle density, g = gravitational acceleration, and V_p = particle volume, with $V_p = (\pi/6)D^3$ for a sphere.

The added mass force F_{AM} is a pressure force that opposes the particle acceleration (Murphy & Hooshiari 1982). The fluid particles displaced by the particle in motion do not return to their previous positions after the particle passes but are shifted to the fluid motion direction. This permanently displaced mass is referred to the added mass (Falkovich 2011).

A particle is set to motion when the force exerted by the fluid exceeds the retarding force. Incipient motion of a single particle mainly depends on its location on the bed, the decisive streamwise velocity acting on it and the corresponding turbulent forces (Fig. 1). When the acting drag force F_D exceeds the retarding Coulomb friction force F_R, the particle changes its state of movement from rest to rolling or sliding motion.

The Coulomb friction force F_R follows

$$F_R = \mu\left(F_G - F_{LG}\right) + G\sin\alpha \tag{5}$$

with μ = Coulomb friction coefficient, and $\mu = \tan\phi_s$, with ϕ_s as submerged angle of repose being $\phi_s \approx 30°$ for sand and gradually increasing to $\phi_s \approx 40°$ for gravel (García 2008). The dynamic friction coefficient for sliding motion is somewhat lower than the static Coulomb friction coefficient due to the fact that a static object provokes a higher resistance than a moving one. The rolling dynamic friction coefficient is calculated as $\mu_r = 2d/D$, with d = particle contact length, and values are more than two orders of magnitude lower than the static sliding friction coefficient (Böge 2006).

At the onset of motion, both the lift force due to particle rotation and the added mass force are absent (García 2008). The critical condition for incipient motion can thus be written as

$$F_R = F_D \tag{6}$$

This simplified particle motion model is basically dependent on the drag coefficient C_D, the slip velocity, e.g. the difference between fluid and particle velocity, and the submerged particle weight.

The drag coefficient C_D is directly dependent on the turbulent flow conditions and varies with the particle Reynolds number R_p. A particle settling in still water will reach a constant terminal settling

velocity once the drag equals the submerged particle weight (García 2008). Therefore, at a certain Reynolds number the drag coefficient C_D becomes a constant. However, exact determination of C_D is challenging, and still a topical research subject. For a sphere in laminar flow with very low particle Reynolds numbers $R_p < 10^{-1}$, where no wake is present behind the sphere, Stokes (1851) found the drag coefficient $C_D = 24/R_p$. Perry & Green (2008) proposed the widely applied constant value $C_D = 0.445 \pm 13\%$ for $10^3 < R_p < 3.5 \times 10^5$. At high Reynolds numbers $R_p > 5 \times 10^5$ Schlichting & Gersten (2003) stated a similar constant value of $C_D = 0.4$.

In the following the particle velocity V_p is analyzed and discussed in detail.

3 DIMENSIONLESS PARAMETERS

To accurately describe particle motion some decisive dimensionless parameters are introduced in the following. The standard parameter to describe the different flow regimes of open channel flow is the Froude number F being the ratio of inertial forces to gravitational forces given by

$$F = \frac{U}{\sqrt{gh}} \tag{7}$$

where h = flow depth. The numerator represents the characteristic flow velocity while the denominator represents the wave celerity computed as $c = (gh)^{0.5}$ for rectangular cross-section. The friction velocity U_* characterizes the shear at the boundary. Herein U_* is calculated using the energy line slope S_e due to nonuniform, but gradually varied flow conditions in the experiments

$$U_* = \sqrt{\frac{\tau_b}{\rho}} = \sqrt{gR_hS_e} \tag{8}$$

with τ_b = boundary shear stress, R_h = hydraulic radius. The relation between the fluid and friction velocity is given by the Chézy coefficient c_z as

$$c_z = \frac{U}{U_*} \tag{9}$$

The widely applied standard parameter to describe sediment motion is the Shields parameter introduced by Shields (1936) as

$$\theta = \frac{U_*^2}{(s-1)gD} \tag{10}$$

The bed roughness is described by the roughness Reynolds number k_s^+

$$k_s^+ = \frac{U_* k_s}{\nu} \tag{11}$$

with k_s as equivalent sand roughness height introduced by Nikuradse (1932, 1933), and ν = kinematic viscosity. Note that in case of gravel bed rivers sediment grains move on top of equally sized grains of diameter D, therefore k_s is in the range of D, thus k_s^+ equals the particle Reynolds number R_p. Herein, the ratio of k_s to D is much lower than unity and varies from $k_s/D = 0.02$–0.06.

4 EXPERIMENTAL SETUP

4.1 *Model flume*

The experiments were conducted in a 0.30 m wide, 0.50 m high and 13.50 m long glass- and PVC-sided concrete lined tilting flume with a maximum discharge of Q = 250 l/s. The coordinates in the streamwise, spanwise and vertical directions are x, y and z (Fig. 2). The discharge was controlled with a magnetic flow-meter and transferred from pressurized to supercritical free surface flow using a VAW jetbox (Schwalt & Hager 1992). The approach flow depth h_o was gate-controlled, and the flow depth h along the flume was measured with both, Ultrasonic Distance Sensors (UDS) and a point gage.

Velocity measurements were carried out by Auel et al. (2014a) using a *Laser Doppler Anemometer* (LDA) system. The measured two-dimensional velocity data show the logarithmic Prandtl-von Kármán type velocity distribution. For each run U_* and k_s were obtained by applying the *log-law* (Nezu and Nakagawa 1993) to the velocity profiles as

$$\frac{U}{U_*} = \frac{1}{\kappa}\ln\left(\frac{z}{z_0}\right) \tag{12}$$

with $\kappa = 0.41$ as the von Kármán constant, and z_0 = zero-velocity level from the channel bed given

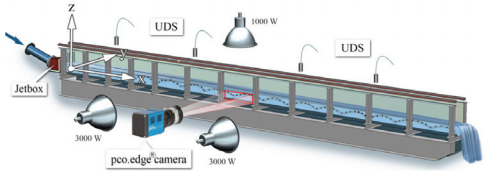

Figure 2. Sketch of model flume.

by Duan (2004) based on Nikuradse (1932, 1933) as

$$z_0 = 0.11\frac{\nu}{U_*} + 0.033k_s \tag{13}$$

This formula is valid in the transitional regime from $5 < k_s^+ < 70$. The average value of k_s found by Auel et al. (2014a) is $k_s = 0.3$ mm (±0.2 mm).

4.2 *Test runs*

The flow was fully developed, supercritical, and both uniform and gradually varied. All test runs were conducted at steady flow conditions at a transitional hydraulically rough regime. Glass spheres were used with diameters D of 5.3, 10.3 and 17.5 mm and corresponding densities ρ_s = 2,530, 2,570 and 2,340 kg/m^3, respectively. Each particle was added separately by hand at the flume center $x = 0.50$ m downstream of the jetbox. The following hydraulic parameters were systematically varied: Bed slope $S_b = 0.01$ and 0.04, $h_o = 50$ and 100 mm, and approach flow Froude number F_o = 1.25, 1.5 to 6.0 (in 0.5 steps). Every test run was repeated $n = 20$ times to allow for a statistical analysis yielding to 2,640 recorded motions of glass spheres. In the present article we focus on one test series implying 33 test runs with $S_b = 0.04$, $h_o = 100$ mm at 11 Froude number variations for all particle sizes.

4.3 *Data recording and image analysis*

Particle motion was recorded using the *pco.edge* scientific CMOS—high speed camera system. The image resolution was 2,560 × 400 pixels corresponding to the area of 1,100 × 200 mm. The frame rate was fixed at 240 fps. The flume was illuminated with 7,000 W lighting in total to allow for a 0.2 ms exposure time. Image processing was carried out by an in-house developed Matlab® Code based on a similar algorithm as applied by Detert and Weitbrecht (2012) for the object detection software Basegrain®. All particles were painted white, whereas the bottom and PVC-wall were black to obtain high-contrast images. Only the large glass spheres were unpainted resulting in a diaphanous particle center. In Figure 3 the single particle tracking steps are presented showing a challenging test run with a large glass sphere to demonstrate the algorithm robustness. The original image was transferred from an 8-bit greyscale (a) into a binary image (b) subtracting the first recorded image containing no particle and applying Otsu's method (Otsu 1979). Then the bed and water level surface (c) were cut. Due to the diaphanous sphere only the particle edges were detected. Thus, the detected pixels were dilated (d) and reduced again (e) by

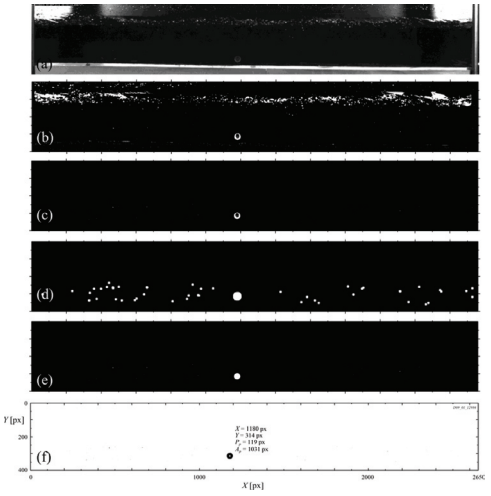

Figure 3. Six particle tracking steps. Exemplary test run with $S_b = 0.01$, $F_o = 4$, $h_0 = 100$ mm, particle diameter $D = 17.5$ mm. a) original 8bit photograph, b) binary black-white image, c) bed and water surface cutting, d) pixel dilation, e) pixel reduction, f) boundary detection.

the same size. As a result, the empty space inside the particle perimeter is filled. Finally the particle boundaries were detected using the Matlab® function *bwboundaries* and the particle properties were obtained (f) using the function *regionprops*. The remaining areas were filtered using a predefined area range for every particle diameter. Small areas with a size of some pixels were thereby deleted. However, if two or more equal-sized areas remained in the figure due to wavy two-phase flow for example, the particle center coordinates of image *i*–1 were used to determine the closest downstream area in figure *i*. The more distant areas were deleted. Finally only one area per image remained. The function *regionprops* provides the center coordinates x and z, the area A, the perimeter P, the major and minor axes a and b and the rotational angle between a and a horizontal line.

As an example, Figure 4 shows characteristic saltating motion of three spheres with diameters $D = 17.5$, 10.3, and 5.3 mm, respectively. Note that the raw images are superimposed by the center coordinates of some 100 consecutive particles.

Herein, the instantaneous horizontal and vertical particle velocities u_i and w_i were calculated between two consecutive recorded images as

$$u_i = \frac{\Delta x}{\Delta t}, w_i = \frac{\Delta z}{\Delta t} \tag{14}$$

where $\Delta t = 1/240$ s is the time difference between the images, and $\Delta x = x_{i+1} - x_i$, and $\Delta z = z_{i+1} - z_i$ as the

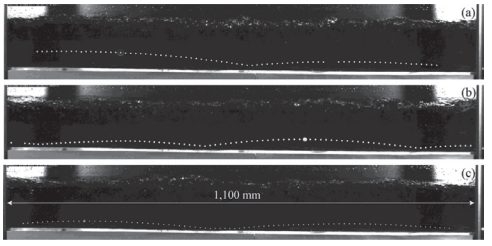

Figure 4. Motion of a single glass sphere. Exemplary test run with $S_b = 0.01$, $F_o = 4$, $h_0 = 100$ mm. a) $D = 17.5$ mm, b) $D = 10.3$ mm, c) $D = 5.3$ mm.

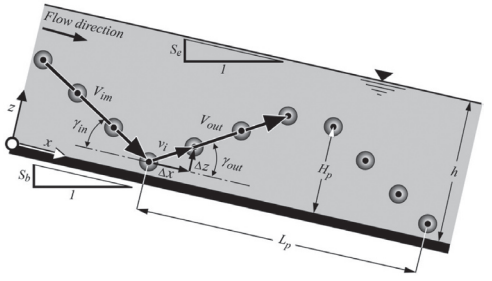

Figure 5. Sketch of particle motion.

horizontal and vertical displacements of the particles, respectively (Fig. 5). The resultant instantaneous velocity v_i is given by its modulus as

$$v_i = \sqrt{u_i^2 + w_i^2} \tag{15}$$

The particle velocity $v_{p,n}$ is defined as the average of all consecutive velocities v_i per single particle within the recorded flume section, and the mean particle velocity V_p is the average of $n = 20$ particles for the same flow condition.

5 EXPERIMENTAL RESULTS

The experimental results show that particles were dominantly transported in saltation mode with minor parts in rolling mode (Auel et al. 2014b). The distinction between rolling motion and saltation was implemented in the algorithm used in the data analysis as follows: if a particle rises and its center exceeds a distance of $0.1D$ away from the bed, the particle changes its mode to saltation. The threshold $0.1D$ was adjusted by trial and error and compared to the visually determined transport mode. A similar approach and threshold value of $0.07D$ were used by Böhm et al. (2006).

The rolling probability for every test condition decreased from 80 to 15% for the large, from 30 to 10% for the medium, and from 10 to 0% for the small-sized spheres with increasing flow intensity. Thus the rolling velocity data for the latter is poor and was neglected if the saltation probability exceeded 95%.

In the range of the investigated flow conditions, almost no difference was observed between the particle rolling velocity V_{roll} and particle saltation velocity V_{sal} and a linearly increasing relationship between these velocities was obtained (Fig. 6). We thus conclude that the particle velocity V_p is quasi-independent from the transport mode.

In general, the particle velocity V_p is expressed as a function of the friction velocity U_* and written as (Abbott & Francis 1977, Bridge & Dominic 1984, Niño et al. 1994)

$$V_p = a \cdot \left(U_* - U_{*c} \right) \tag{16}$$

with a being a constant. Figure 7 shows V_p as a function of U_* for all 33 test runs and reveals that V_p increases linearly with U_*. From the linear data fit, the critical value U_{*_c} is determined. The correlation is high ($R^2 = 0.99$) and follows

$$V_p = 25 \cdot \left(U_* - 0.027 \right) \tag{17}$$

The critical friction velocity is $U_{*_c} = 0.027$ m/s and the constant is $a = 25$. The determination of U_{*_c} is achieved through an extrapolation of the experimental data. As the onset of motion was not the project focus, no experiment was made at low flow intensities. However, in the following it is shown that the obtained value corresponds well with comparable literature data.

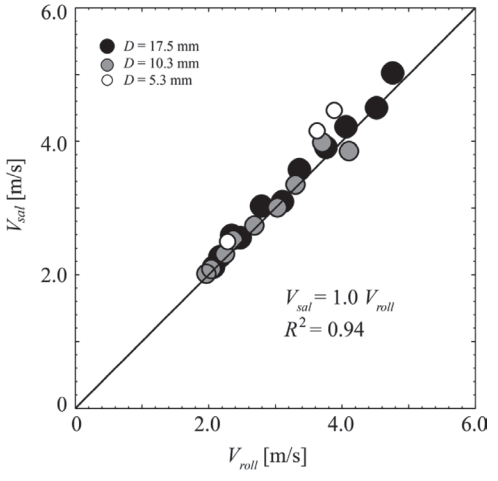

Figure 6. Particle saltation velocity V_{sal} as a function of rolling particle velocity V_{roll}. Particles with less than 5% rolling probability omitted.

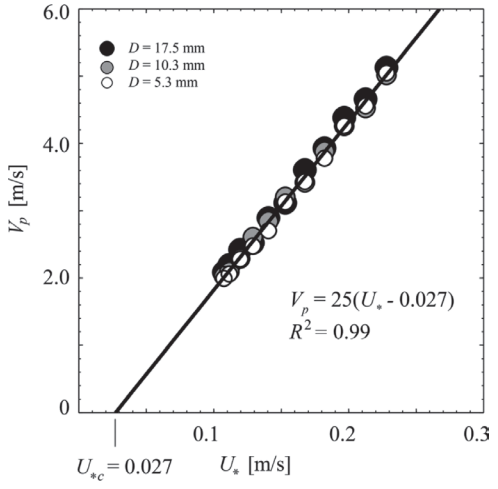

Figure 7. Particle velocity V_p as a function of friction velocity U_*.

Only a slight effect of the particle diameter on the $V_p \sim U_*$ relation is observed. Large particles travel in average approximately 3% and 5% faster than the medium and small ones, respectively. The values of a obtained from erodible, movable bed conditions vary around $a \approx 5$ (Niño et al. 1994, Lajeunesse et al. 2010), while they vary around $a = 10$~15 on rough fixed bed conditions (Francis 1973, Abbott and Francis 1977, Mantz 1980).

However, the present data deviates and doubles these values. This is attributed to the differences in the flow to friction velocity ratio which is expressed by the dimensionless Chézy coefficient c_z (Eq. 10). Standard values of c_z observed for movable bed experiments and gravel bed rivers vary around $c_z \approx 10$ (Lajeunesse et al. 2010). Auel et al. (2014a) found higher values for the present experimental flow conditions ($c_z = 21 \pm 1.3$) due to both the transitional rough bed and low relative roughness ($k_s/h = 0.02$–0.03). Similar values of c_z, i.e. 21~22, have been documented by Nezu and Rodi (1986) for an open channel flow over a smooth bed with $F_o = 1.1$~1.24. Note that these values are double or even higher compared to gravel bed rivers and thus explain the difference between the a values.

Applying the critical friction velocity $U_{*_c} = 0.027$ m/s to Equation 11 leads to critical Shields parameters of $\theta_c = 0.009$, 0.005, and 0.003 for $D = 5.3$, 10.3 and 17.5 mm, respectively. An averaged critical Shields parameter is obtained applying an average sphere diameter of $D_m = 11.0$ mm with an average density of 2,480 kg/m^3 leading to $\theta_{cm} = 0.005$. These values are an order of magnitude lower compared to alluvial river bed data due to the fixed transitional rough bed. Other fixed smooth and transitional bed data yield $\theta_c = 0.007$ as stated by Chatanantavet et al. (2013), indicating that the obtained θ_c is in a good agreement with literature data, and thus the value of U_{*_c} is reasonable.

Figure 8 shows a normalized plot based on Lajeunesse et al. (2010). V_p presented in Figure 7 is scaled with the particle settling velocity V_s given by Ferguson & Church (2004) as

$$V_s = \frac{(s-1)gD^2}{C_1\nu + \left(0.75C_2(s-1)gD^3\right)^{0.5}} \tag{18}$$

where $C_1 = 18$ and $C_2 = 0.4$ for smooth spheres. Additionally the published data from Fernandez Luque & van Beek (1976), Abbott & Francis (1977), Lee & Hsu (1994), Niño et al. (1994), and Lajeunesse et al. (2010) are plotted for both movable and fixed rough beds.

All data show a linearly increasing relationship between V_p/V_s and U_*/V_s, but the magnitude of the present data significantly differ from the other data primarily due to the low ratio k_s/D. For similar U_*/V_s the scaled particle velocities from the present experiments are around 2 and 5 times higher than those from the published data. In general, the data over movable bed experiments (Niño et al. 1994, Lajeunesse et al. 2010) show lower relative particle velocities compared to data over fixed rough bed experiments (Abbott & Francis 1977, Lee & Hsu 1994).

The above mentioned large value of the flow to friction velocity ratio of $c_z \approx 21$ in the present study compared to $c_z \approx 10$ for rough beds is considered as

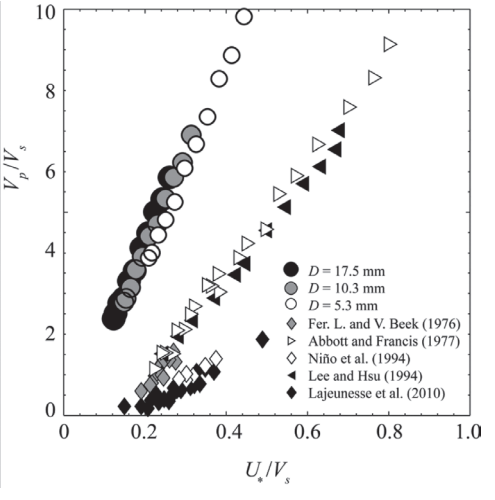

Figure 8. Normalized particle velocity V_p/V_s as a function of normalized friction velocity U_*/V_s. External data taken from Lajeunesse et al. (2010).

the main reason for the deviating data observed in Figure 8. Thus normalization with the flow velocity (or Froude number) would merge the data sets, which is shown in the following.

Furthermore, different particle diameter, density and shape may also have an effect on the deviation in Figure 8. The larger the particle the more it is exposed to the flow, and the more it is accelerated by the streamwise flow component due to the logarithmic velocity profile (Eq. 13).

Figure 9 shows the particles velocities normalized by the wave celerity $c = (gh)^{0.5}$ as proposed by Chatanantavet et al. (2013) as a function of the Froude number F. The data sets of Abbott & Francis (1977), Niño et al. (1994), and Lee & Hsu (1994) are included in Figure 9. Note that the data from Fernandez Luque & van Beek (1976), and Lajeunesse et al. (2010) were not added due to a lack of flow velocity data. The data sets merge and collapse with the present data due to the fact that F represents the flow velocity, thus neglecting the above discussed deviation in the friction velocity.

The normalized particle velocity increases linearly with F and may be approximated as

$$\frac{V_p}{\sqrt{gh}} = 1.1\,F - 0.7 \text{ for } 0.5 \le F \le 5.0 \qquad (19)$$

The overall data correlation is excellent ($R^2 = 0.99$). However, in the subcritical flow region, the scatter is slightly higher due to the roughness effect in the added studies. With increasing flow intensity, i.e. Froude number, the deviation decreases as the particles change to the saltation mode and the bed contact decreases. Note that since plotting all data in a dimensional form, i.e. V_p versus U_* yields a strong correlation as shown in Figure 7, and the relation between U_* and U is evidently given by c_z, the strong correlation in Figure 9 is not an artifact of the normalization using the wave celerity c appearing in both the dependent and independent variables (Chatanantavet et al. 2013).

As a result, all added external data sets complement the present data providing a linear fit valid for a large Froude number range.

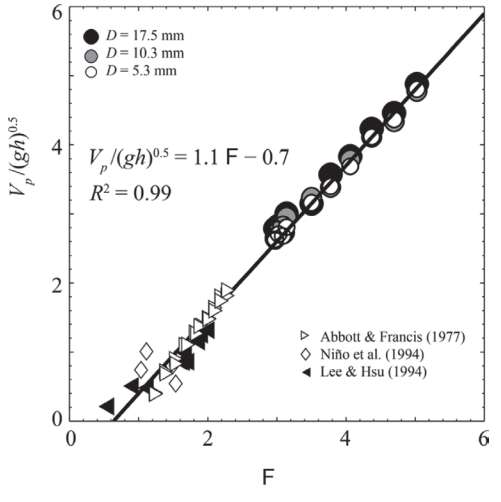

Figure 9. Normalized particle velocity $V_p/(gh)^{0.5}$ as a function of Froude number F.

6 CONCLUSIONS

Single glass sphere motion recordings were conducted in a transitional rough bed open channel at steady, supercritical, and both uniform and gradually varied flow similar to hydraulic conditions present in sediment bypass tunnels. The relative roughness varied from k_s/h = 0.02–0.03, and particles move over a bed with roughness elements more than an order of magnitude smaller than its diameter. The results of the data analysis on 660 recorded motions of glass spheres out of 2,640 have been presented.

The dominant transport mode in the present experiments was saltation with minor parts in rolling motion. The particle velocities were determined for a wide range of test runs varying the Froude number and particle diameter. A linear relationship was found for rolling and saltating particle velocities. Thus the particle velocity is independent on the transport mode in the range of the investigated hydraulic conditions. Regarding particle saltation motion, the particle velocities show a linear relationship with the friction velocity or Froude number quasi-independent on the particle diameter.

Comparison between literature data over movable bed and the present data reveals a significant effect of relative bed roughness on the particle velocity. The particle velocities normalized by the particle settling velocity from the present experiments are around 2 to 5 times higher than those from the published data when plotted as a function of the friction velocity. This is attributed to the fact that for the same flow velocity the friction velocity is affected by bed roughness, channel width to water depth ratio, i.e. 2D and 3D flow conditions, and Froude number. Therefore, scaling the particle velocities with the wave celerity and plotting them as a function of the Froude number yields a better collapse of the present and the former data. Taking into account that the present experiments were carried out at much higher Froude numbers than those reported in the literature and that the results

agree with most of the findings in the literature, the dynamics and the characteristics of particle bedload motion and the corresponding particle velocities presented with adequate scaling appear to be quasi-universal.

ACKNOWLEDGEMENTS

The authors would like to acknowledge the financial support of *swisselectric* research and the Swiss Federal Office of Energy.

REFERENCES

Abbott, J.E. & Francis, J.R.D. 1977. Saltation and suspension trajectories of solid grains in a water stream. *Philos. Trans. Royal Society of London A* 284(1321): 225–254.

Ancey, C., Bigillon, F., Frey, P., Lanier, J. & Ducret, R. 2002. Saltating motion of a bead in a rapid water stream. *Physical Review E*, 66(3).

Ancey, C., Bigillon, F., Frey, P. & Ducret, R. 2003. Rolling motion of a bead in a rapid water stream. *Physical Review E*, 67(1).

Ancey, C., Davidson, A.C., Böhm, T., Jodeau, M. & Frey, P. 2008. Entrainment and motion of coarse particles in a shallow water stream down a steep slope. *Journal of Fluid Mechanics* 595: 83–114.

Auel, C., Albayrak, I. & Boes, R.M. 2014a. Turbulence characteristics in supercritical open channel flows: Effects of Froude number and aspect ratio. *Journal of Hydraulic Engineering* 140(4), 04014004, 16p.

Auel, C., Albayrak, I. & Boes, R.M. 2014b. Laborversuche über die Partikelbewegung in schiessendem Abfluss ('Laboratory experiments on particle motion in supercritical flows'). *Proc. Intl. Symposium "Wasser- und Flussbau im Alpenraum"*, ETH Zurich, Switzerland (in German).

Auel, C. & Boes, R.M. 2012. Sustainable reservoir management using sediment bypass tunnels. Proc. *24th ICOLD Congress*, Kyoto, Japan, Q92(R16): 224–241.

Auel, C. & Boes, R.M 2011. Sediment bypass tunnel design – review and outlook. *Proc. 79th ICOLD Annual Meeting*. Dams and reservoirs under changing challenges (A.J. Schleiss and R.M. Boes, eds.), CRC Press/Balkema, Leiden, The Netherlands: 403–412.

Böge, A. 2006. Formeln und Tabellen zur Technischen Mechanik ('Formulas and tables on technical mechanics'). 20th edition, *Vieweg*, Wiesbaden, Germany (in German).

Böhm, T., Frey, P., Ducottet, C., Ancey, C., Jodeau, M. & Rebou, J.-L. 2006. Two-dimensional motion of a set of particles in a free surface flow with image processing. *Experiments in Fluids* 41, 1–11.

Bridge, J.S. & Dominic, D.F. 1984. Bed-load grain velocities and sediment transport rates. *Water Resources Research* 20(4): 476–490.

Chatanantavet, P., Whipple, K.X., Adams, M.A. & Lamb, M.P. 2013. Experimental study on coarse grain saltation dynamics in bedrock channels. *Journal of Geophysical Research: Earth Surface* 118: 1–6.

Chepil, W.S. 1958. The use of evenly spaced hemispheres to evaluate aerodynamic forces on a soil surface. *Transactions of the American Geophysical Union* 39(3): 397–404.

Detert, M. & Weitbrecht, V. 2012. Automatic object detection to analyze the geometry of gravel grains – a free stand-alone tool. *Proc. River Flow,* R.M. Muños (Ed.), Costa Rica: 595–600.

Duan J.G. 2004. Simulation of flow and mass dispersion in meandering channels. *Journal of Hydraulic Engineering* 130(10): 964–976.

Falkovich, G. 2011. Fluid mechanics (a short course for physicists). *Cambridge University Press*, UK.

Ferguson, R.I. & Church, M. 2004. A simple universal equation for grain settling velocity. *Journal of Sedimentary Research* 74(6): 933–937.

Fernandez Luque, R. & Van Beek, R. 1976. Erosion and transport of bed-load sediment. *Journal of Hydraulic Research* 14(2): 127–144.

Francis, J.R.D. 1973. Experiments on motion of solitary grains along bed of a water-stream. Proc. of the *Royal Society of London A* 332(1591): 443–471.

García, M.H. 2008. Sedimentation Engineering. *ASCE Manuals and Reports on Engineering Practice* 110, American Society of Civil Engineers, USA.

Hu, C. & Hui, Y. 1996. Bed-load transport. I: Mechanical characteristics. *Journal of Hydraulic Engineering* 122(5): 245–254.

Julien, P.Y & Bounvilay, B. 2013. Velocity of Rolling Bed Load Particles. *Journal of Hydraulic Engineering* 139(2): 177–186.

Lajeunesse, E., Malverti, L. & Charru, F. 2010. Bed load transport in turbulent flow at the grain scale: Experiments and modeling. *Journal of Geophysical Research: Earth Surface* 115(F04001): 16p.

Lee, H.Y. & Hsu, I.S. 1994. Investigation of saltating particle motions. *Journal of Hydraulic Engineering* 120(7): 831–845.

Mantz, P.A. 1980. Low sediment transport rates over flat beds. *Journal of the Hydraulics Division* ASCE 106(HY7): 1173–1190.

Meland, N. & Norrman, J.O. 1966. Transport velocities of single particles in bed-load motion. *Geografiska Annaler, Series A* 48(4): 165–182.

Murphy P.J. & Hooshiari H. 1982. Saltation in water dynamics. *Journal of the Hydraulics Division* 108(11): 1251–1267.

Nezu, I. & Nakagawa, H. 1993 Turbulence in open-channel flows. *IAHR Monograph*, Balkema, Rotterdam, The Netherlands.

Nezu, I. & Rodi, W. 1986. Open-channel flow measurements with a laser Doppler anemometer. Journal of Hydraulic Engineering, 112 (5): 335–355.

Nikuradse, J. 1933. Strömungsgesetze in rauhen Rohren ('Flow laws in rough ducts'). *Forschungsheft* 361, VDI-Verlag GmbH, Berlin, Germany (in German).

Nikuradse, J. 1932. Gesetzmäßigkeiten der turbulenten Strömung in glatten Rohren ('Laws of turbulent flow in smooth ducts'). *Forschungsheft* 356, VDI-Verlag GmbH, Berlin, Germany (in German).

Niño, Y., Garcia, M. & Ayala L. 1994. Gravel saltation 1. Experiments. *Water Resources Research* 30(6): 1907–1914.

Otsu, N. 1979. A threshold selection method from gray-level histograms. *IEEE Transactions on Systems, Man, and Cybernetics* 9(1), 62–66.
Perry, R.H. & Green, D.W. 2008. Perry's chemical engineers' handbook. 8th ed., *McGraw-Hill*, New York, USA.
Rubinow, S.I. & Keller, J.B. 1961. The transverse force on a spinning sphere moving in a viscous fluid. *Journal of Fluid Mechanics* 11(3), 447–459.
Schlichting, H. & Gersten, K. 2003. Boundary layer theory. 8th ed. *Springer*, Berlin, Germany.
Schwalt, M. & Hager, W.H. 1992. Die Strahlbox ('The jetbox'). *Schweizer Ingenieur und Architekt* 110(27/28): 547–549 (in German).
Shields, A. 1936. Anwendung der Aehnlichkeitsmechanik und der Turbulenzforschung auf die Geschiebebewegung ('Application of similarity principles and turbulence research to bed-load movement'). *Mitteilungen der Preussischen Versuchsanstalt für Wasserbau und Schiffbau* Heft 26, Berlin, Germany (in German).
Stokes, G.G. 1851. On the effect on internal friction of fluids on the motion of pendulums. *Transactions of the Cambridge Philosophical Society* 9, 8–106.
Sumi, T., Okano, M. & Takata, Y. 2004. Reservoir sedimentation management with bypass tunnels in Japan. *Proc. 9th Int. Symposium on River Sedimentation*, Yichang, China: 1036–1043.
van Rijn, L.C. 1984. Sediment transport, Part I: Bed load transport. *Journal of Hydraulic Engineering* 110(10): 1431–1456.